Multiple Optimal Depth Predictors Analysis (MODPA) for River Bathymetry: Findings from Spectroradiometry, Simulations, and Satellite Imagery

Milad Niroumand-Jadidi*[a, b, c], Alfonso Vitti [a] and David R. Lyzenga [d]

[a] *Department of Civil, Environmental, and Mechanical Engineering, University of Trento, Via Mesiano, 77 - 38123 Trento, Italy. Email: m.niroumand@unitn.it*

[b] *Department of Biology, Chemistry, and Pharmacy, Freie Universität Berlin, Altensteinstraße 6, 14195 Berlin, Germany.*

[c] *Leibniz-Institute of Freshwater Ecology and Inland Fisheries, Müggelseedamm 310, 12587 Berlin, Germany*

[d] *Department of Naval Architecture and Marine Engineering, College of Engineering, University of Michigan, 115 NAME Bldg., 2600 Draper Dr. Ann Arbor, MI 48109-2145, Michigan, USA.*

Abstract:

Remote mapping of bathymetry can play a key role in gaining spatial and temporal insight into fluvial processes, ranging from hydraulics and morphodynamics to habitat conditions. This research introduces Multiple Optimal Depth Predictors Analysis (MODPA), which combines previously developed depth predictors along with additional predictors derived from the intensity component of the HSI color space transformation. MODPA empirically selects a set of optimal predictors among all candidates utilizing partial least squares (PLS), stepwise, or principal component (PC) regression models. The primary focus of this study was on shallow (< 1 m deep) and clearly flowing streams where substrate variability could have a pronounced effect on depth retrieval. Spectroscopic experiments were performed under controlled conditions in a hydraulic laboratory to examine the robustness of bathymetry models with respect to changes in bottom type. Further, simulations from radiative transfer modeling were used to extend the analysis by isolating the effect of inherent optical properties (IOPs) and by investigating the performance of bathymetry models in optically complex and deeper streams. The bathymetry of the Sarca River, a shallow river in the Italian Alps, was mapped using a WorldView-2 (WV-2) image, for which we evaluated the atmospheric compensation (AComp) product. Results indicated the greater robustness of multiple-predictor models particularly MODPA rather than single-predictor models, such as Optimal

Band Ratio Analysis (OBRA), with respect to heterogeneity of bottom types, IOPs, and atmospheric effects. The HSI intensity component enhanced the accuracy of depth retrieval, particularly in optically-complex waters and also for low spectral resolution imagery (e.g., GeoEye). Further, the enhanced spectral resolution of WV-2 imagery improved bathymetry retrieval compared to 4-band GeoEye data.

***Keywords*:** bathymetry, river, Lyzenga model, ratio model, depth predictors, spectroscopy, WorldView-2, atmospheric compensation (AComp)

1- Introduction

Remote sensing techniques provide an alternative to traditional field-based measurements and have the potential to enhance our understanding of fluvial systems by providing spatially and temporally explicit information (Marcus and Fonstad, 2008; Carbonneau et al., 2012; Legleiter and Overstreet, 2012; Niroumand-Jadidi and Vitti, 2016; Shintani and Fonstad, 2017; Niroumand-Jadidi and Vitti, 2017a). The recent integration of remote sensing and river sciences has emerged as a growing research field termed "fluvial remote sensing" (Marcus and Fonstad, 2010; Carbonneau et al., 2012). Advancements in sensors, such as water-penetrating, green-wavelength light detection and ranging (LiDAR), or platforms, such as unmanned aerial vehicles (UAVs), have recently provided new tools for characterizing fluvial systems (Kinzel et al., 2013; Flener et al., 2013; Shintani and Fonstad, 2017). However, green LiDAR observations are mainly feasible by means of low-altitude platforms (e.g., manned aircrafts), which leads to a lower spatial and temporal coverage compared to optical sensing by means of satellites. Furthermore, the application of green LiDAR in riverine environments is hindered by low point density of observations and also the confusion among laser returns from the water surface, water column, and riverbed (Legleiter and Overstreet, 2012; Kinzel et al., 2013). UAVs offer the potential for higher spatial and temporal resolution, but at the cost of spatial coverage. In this context, passive optical remote sensing aboard airborne and spaceborne platforms remains a broadly applicable means of characterizing a wide range of attributes in fluvial systems, including bathymetry (Legleiter and Overstreet, 2012; Niroumand-Jadidi and

Vitti, 2016), substrate type and composition (Legleiter et al., 2016), grain size (Carbonneau et al., 2004; Niroumand-Jadidi and Vitti, 2017b), and hydromorphological units (Legleiter et al., 2004).

Bathymetry is one of the key applications of remote sensing to fluvial systems that facilitates understanding river form, process, and function (Shintani and Fonstad, 2017). Information on water depth can play a valuable role in mapping in-stream habitats (Carbonneau et al., 2012; Hugue et al., 2016), parameterization and analysis of hydro-morphological processes (Bryant and Gilvear, 1999; Flener et al., 2012), and river management (Fonstad and Marcus, 2005; Legleiter and Overstreet, 2012). Optical sensors onboard aerial and satellite platforms have long been used for studying shallow coastal environments (Lyzenga, 1978; Lyzenga, 1981, Philpot, 1989; Dierssenet al., 2003; Louchard et al., 2003; Lesser and Mobley, 2007). Because of their smaller spatial scales, fluvial systems have mostly utilized aerial imagery to derive bathymetric data (Winterbottom and Gilvear, 1997; Jordan and Fonstad, 2005; Walther et al., 2011; Legleiter, 2013). With recent enhancements in spatial resolution of satellite imagery, mapping river bathymetry from space is receiving more interest due to larger spatial coverage and higher temporal resolution of satellite sensors than those onboard aerial platforms. Legleiter and Overstreet (2012) performed a feasibility assessment of mapping the bathymetry of gravel-bed rivers from space using WorldView-2 (WV-2) imagery.

The theoretical basis for optical remote sensing of bathymetry in riverine environments is built upon research conducted in optically shallow coastal environments (Legleiter et al., 2004; Legleiter et al., 2009). Bathymetric techniques fall into two main approaches: through-water photogrammetry (Fryer, 1983; Westaway et al., 2001) and spectrally based analysis (Lyzenga, 1978; Lee et al., 1998). Through-water photogrammetry utilizes stereo imagery to produce a digital elevation model by accounting for refraction of light at the air-water interface (Westaway et al., 2001; Lane et al., 2010). One particular type of photogrammetric approach known as Structure from Motion (SfM) has received growing interest for measuring bathymetry and characterizing riverbed topography (Woodget et al., 2015; Dietrich, 2017). SfM is capable of reconstructing three-dimensional geometry using multiple overlapping images taken from a wide range of angles (Shintani and Fonstad, 2017). Spectrally based approaches to deriving bathymetric data can be divided into physics-based and empirical models (Brando et al., 2009; Dekker et al., 2011). The first rely on inversion of radiative transfer models and account for the physics of how light interacts with the water surface, water-column, and bottom (Lee et al., 1998; Lee et al., 1999; Lesser and Mobley, 2007; Brando et al., 2009), while the latter provide regression-based predictions of bathymetry (Lyzenga, 1978; Philpot, 1989).

The seminal work of Lyzenga (1978, 1981) provides a basis for empirical retrieval of water depths from optical imagery, which was the focus of this research. Lyzenga's model assumes a linear relation between an image-derived quantity (X) and the water depth (d), where X is a predictor obtained from log-transformation of image values in a given spectral band. Multiple regression (Lyzenga, 1985; Lyzenga et al., 2006) and ratio methods (Stumpf et al., 2003) have been demonstrated to enhance the robustness of bathymetry retrieval with respect to substrate variability and water quality heterogeneity. The first employs multiple spectral bands to perform a multiple linear regression between image-derived predictors (X) and water depths (d) while the latter model considers a log-transformed band ratio as a single predictor of water depth. More recently, Optimal Band Ratio Analysis (OBRA) was introduced to identify the pair of bands, among all possible pairs, for which the ratio model yields the strongest correlation with water depth (Legleiter et al., 2009). Each of these types of predictors has been reported as optimal in different case studies (Legleiter et al., 2012; Bramante et al., 2013; Jawak and Luis, 2016).

Further development of new techniques is required to systematically select and combine a set of predictors that provide robust retrievals in the presence of all the complicating factors that might impact depth retrieval (e.g., variations in bottom types, IOPs and water-surface roughness). We pursued five main objectives in this study:

(1) Developing a new approach called Multiple Optimal Depth Predictors Analysis (MODPA) for bathymetry retrieval. This method seeks to identify and incorporate optimal depth predictors among all the possible Lyzenga and ratio predictors as well as additional predictors from color space transformation.

The selection of optimal predictors was performed using several feature selection methods including stepwise, partial least square (PLS), and principal component (PC) regressions;

(2) Assessing the robustness of the proposed MODPA compared to existing models with respect to heterogeneity in substrate types, IOPs, and atmospheric effects. Bathymetry models were comprehensively examined using spectroscopic experiments, radiative transfer simulations, and WV-2 imagery. The spectroscopic experiments were conducted under controlled conditions in a hydraulic laboratory and involved collecting a set of spectra in a range of water depths with variable substrates. The effects of IOPs, as influenced by chlorophyll-a (Chl-a), suspended sediment concentration (SSC), and colored dissolved organic matter (CDOM), were isolated using the simulated data. Moreover, we considered an optically complex testing scenario where bottom type and IOPs were both allowed to vary;

(3) Examining the performance of the proposed MODPA method for bathymetry mapping of the Sarca River, a shallow and narrow alpine river in Italy, using WV-2 imagery. This analysis quantified the effectiveness of MODPA compared to other models in the spectrally complex environment of a real case study. Different strategies were considered for the validation of results including an approach built upon comparison of image-derived depths with the estimates based on principles of river hydraulics;

(4) Assessing the effect of atmospheric correction on bathymetry retrieval of the Sarca River, which is an important consideration due to the low reflectivity of water bodies and accordingly sizable contribution of the atmosphere to the total at sensor radiance (Gitelson and Kondratyev, 1991; Mouw et al., 2015). The newly released surface reflectance product of DigitalGlobe (2016), called atmospheric compensation (AComp), was assessed to understand the robustness of bathymetric models with respect to atmospheric effects;

(5) Assessing the efficacy of WV-2 sensor's additional spectral bands compared to traditional high resolution satellite imagery (HRSI, less than 5 m pixel size) with only four bands such as GeoEye.

2- Bathymetry from Optical Imagery

In the context of optical remote sensing of water bodies, the total radiance reaching the sensor at a given wavelength λ, $L_T(\lambda)$, consists of four main components: upwelling radiances from the bottom, $L_b(\lambda)$, water column, $L_c(\lambda)$, and surface of the water body, $L_s(\lambda)$, as well as the atmospheric path radiance, $L_p(\lambda)$. These components are summarized in the following equation (Legleiter et al., 2004; Legleiter et al., 2009):

$$L_T(\lambda) = L_b(\lambda) + L_c(\lambda) + L_s(\lambda) + L_p(\lambda) \quad (1)$$

Aside from $L_p(\lambda)$, each of these radiance components can be associated with a specific property of the water body. For instance, the surface-reflected component of the radiance can be linked to the roughness of the water surface, which in turn is a function of local hydraulics in riverine environments and can potentially reveal information about flow velocity (Overstreet and Legleiter, 2017; Legleiter et al., 2017). Information on bathymetry is embedded in the bottom-reflected radiance component, which is affected not only by water depth but also by bottom type and indirectly by water column optical properties (Lee et al., 1998; Stumpf et al., 2003; Legleiter et al., 2009). Thus, it is essential to isolate the radiance component of interest or to reduce the effect of other extraneous components in order to retrieve the desired parameter, which in this study is the water depth.

Lyzenga's model (1978, 1981) is built upon the Beer-Lambert law, which describes the exponential attenuation of light travelling through the water column. This model includes a deep-water correction term, $L_w(\lambda)$, equated with the radiance observed over optically-deep water, to account for the radiance scattered from the water column, water surface, and atmosphere (Eq. 2).

$$L_w(\lambda) = L_c(\lambda) + L_s(\lambda) + L_p(\lambda) \quad (2)$$

The bottom-reflected radiance can be considered negligible for optically-deep waters. Therefore, subtracting $L_w(\lambda)$ from all water pixels leaves the bottom-reflected radiance, which contains bathymetry information. According to Lyzenga's model, the water depth (*d*) depends linearly on the predictor (*X*) derived from image values in a given spectral band (Eqs. 3 and 4).

$$X = \ln\left(L_T(\lambda) - L_w(\lambda)\right) \quad (3)$$

$$d = aX + b \quad (4)$$

Note that deep-water correction required for Lyzenga's model has been demonstrated to be negligible for shallow rivers (Mumby and Edwards, 2000; Flener et al., 2012; Flener, 2013). This is mainly because the bottom signal is the dominant component of radiance reaching the sensor, particularly if the image has been atmospherically corrected. Therefore, there is low probability to approach to the deep-water signal in shallow and clear rivers (Legleiter et al., 2009). Note that type of the substrate is also an important factor influencing the total water-leaving radiance. For instance, depth retrieval in very shallow waters could be hindered by the presence of a dark, low-reflectance substrate that absorbs most of the downwelling radiance. However, this would be a rare case where the bottom-reflected radiance is not sufficient to propagate through the thin water column in riverine environments. The unknown parameters (a, b) can be estimated by means of a simple regression between X and in-situ depths (d). However, these parameters depend on the IOPs of the water column and the bottom reflectance, which might vary within a given scene. To deal with these problems, a linear combination of the predictors (X_i) derived from multiple (n) spectral bands (Eq. 5) has been suggested for depth estimation (Lyzenga et al., 2006).

$$d = \sum_{i=1}^{n} a_i X_i + b \quad (5)$$

Note that water-surface roughness and accordingly surface-reflected radiance can also vary significantly within a given river channel on small spatial scales (Legleiter et al., 2009). These effects cause variations in near-infrared bands, which do not contain significant bottom-reflected signals because of strong attenuation of near-infrared light. Thus, scaled versions of the near-infrared bands can be instrumental for enhancing the robustness of depth retrieval with respect to variations in water surface roughness, as well as atmospheric effects (Lyzenga et al., 2006; Kay et al., 2009).

Stumpf et al. (2003) proposed using a ratio model for depth retrieval to mitigate the undesirable effect of variations in bottom reflectance (Eq. 6).

$$X = ln\left[\frac{L_T(\lambda_1)}{L_T(\lambda_2)}\right] \tag{6}$$

The ratio model relies on the fact that different substrates at the same depth have approximately equal values of the ratio between total radiances at two different wavelengths. Such a ratio can be used as a robust depth predictor with respect to substrate variability (Stumpf et al., 2003; Flener, 2013). Note that Equation 6 is a special case of Equation 5, with n = 2 and $a_2 = -a_1$. So this method is similar to that of Lyzenga, but does not involve deep-water correction. Legleiter et al. (2009) extended the idea of the ratio model in the form of OBRA. This model examines all the possible pairs of bands to identify the pair that provides the highest coefficient of determination (R^2) in a regression of X against d.

Bathymetric models originally developed for coastal environments have only recently been translated to fluvial systems, particularly using HRSI (Legleiter and Overstreet, 2012). The key distinction between coastal and riverine environments is the thinner water-column in rivers. Therefore, a relatively high contribution from the river substrate and a relatively low contribution from the water column can be expected, especially in shallow and clearly flowing streams. Although this is advantageous for depth retrieval due to having stronger bottom-reflected radiance, the pronounced effect of substrate variability complicates depth retrieval. Moreover, as mentioned before, highly variable water-surface roughness in fluvial systems can induce additional challenges. Therefore, development of robust methods is needed to produce reliable and consistent bathymetric maps for large spatial extents using optical imagery.

3- Multiple Optimal Depth Predictors Analysis (MODPA)

Existing bathymetric models employ one or more Lyzenga predictors or a single ratio predictor. Although OBRA identifies the optimal ratio predictor, the model is based on a sole ratio predictor. The selection between predictor types (Lyzenga or ratio) can be challenging in practice, as the results of previous studies indicated that each type of predictor can possibly lead to more accurate results than the other, depending on the case study. For instance, Jawak and Luis (2016) reported that the Lyzenga model derived the bathymetry of a shallow lake (depth < 8 m) more precisely (with 15% higher R^2 and 0.98 m lower RMSE) than the ratio model using WV-2 imagery. Bathymetry models that rely on a simple regression (e.g., OBRA) attempt to explain the dependent variable (i.e., depth) using only one predictor; other informative predictors might be neglected.

This research aimed to integrate previously developed depth predictors by initially considering all of the possible Lyzenga and ratio predictors rather than relying upon only one of the predictor types. In addition, we considered some additional predictors derived from the RGB to HSI (hue, saturation, intensity) color space transformation. More specifically, the intensity component of the HSI space (hereafter called intensity) was added to the original image feature space and included as a potential predictor along with the associated Lyzenga and ratio predictors. The intensity (I) component refers to the total brightness or luminance of the pixels, which is associated with the human perception of brightness (Carper et al., 1990). The intensity component would potentially contribute to depth retrieval because the overall brightness of image pixels is influenced by the optical properties of the water body (Stumpf et al., 2003), which provides a physical basis for considering intensity components as candidate depth predictors. However, as a general rule in regression analysis, new features created through transformation of the original spectral data can provide a better discriminative ability but might not have a clear physical meaning (Markovitch and Rosenstein, 2002; Qian et al., 2012). Note that the color space transformation can be applied to each combination of three spectral bands so that several intensity bands can be added to the feature space (e.g., four intensity bands can be derived for a 4-band GeoEye image). A multiple regression approach was then considered to retain and exploit most of the variability of the predictors. However, making use of all the predictors can pose the problem of overfitting (Howley et al., 2006). Furthermore, high dimensional predictors can invite redundant or correlated predictors which can lead to degradation of regression model's prediction accuracy (Reunanen, 2003; Howley et al., 2006). For example, 36 initial predictors can be derived from 8-band WV-2 imagery (8 Lyzenga predictors and 28 ratio predictors), and this number will increase by intensity predictors. Therefore, performing a dimensionality reduction on all the candidate predictors is essential. This study attempted to select the optimal predictors by using three different regression methods: partial least squares (PLS), stepwise, and principal components (PC). The resultant optimal predictors can then be a combination of Lyzenga, ratio, and intensity predictors.

Stepwise regression is a systematic method for adding and removing terms (predictors) from a linear model based on their statistical significance in explaining the response variable. Stepwise regression uses the p-value of an F-statistic to test models with and without a potential term at each step. PC and PLS are both regression methods that construct new predictors called components as linear combinations of the original predictors. A subset of components then can be selected as optimal predictors in such a way as to keep most of the variability of the original predictors. The number of components can be chosen by looking at the percent of variance explained in the response variable as a function of the number of components. However, PC creates the components without considering the response variable (i.e., depth) while PLS takes the response variable into account (Haenlein and Kaplan, 2004; Matlab, 2018). The PLS regression optimizes the prediction power of the model by simultaneous implementation of dimensionality reduction and regression (Haaland and Thomas, 1988). This means that PLS minimizes the dimensionality of the data while maximizing the covariance between predictor and response variables. A detailed description of the PLS regression is given by Wold et al. (2001). These methods provide powerful modeling tools to deal with large number of predictors when the collinearity among the variables is strong (Abdi, 2003; Li et al., 2014).

4- Hydraulically Assisted Assessment of Bathymetry (HAAB)

In previous studies, bathymetry models were assessed mainly by reserving samples selected at random from in-situ or simulation data (Legleiter et al., 2004; Legleiter et al., 2009). However, the number of field measured samples might not be sufficient for both calibration and validation of models. Moreover, assessment of the depth estimates would not be feasible in reaches not covered during the field survey. In this study, along with the traditional assessment method, we have used an additional approach, which integrates some basics of river hydraulics to estimate independent water depths for accuracy assessment. Fonstad and Marcus (2005) introduced hydraulically assisted bathymetry (HAB), which determines cross-sectional depths based on principles of open channel flow in order to calibrate the bathymetry model in the absence of in-situ data. We have used the same model but for the assessment of depth estimates, which is termed, hereafter, as hydraulically assisted assessment of bathymetry (HAAB).

The basic formula of discharge (Eq. 7) and the flow resistance equation of Manning (Eq. 8) form the basis of the HAB model (Fonstad and Marcus, 2005).

$$Q = W\bar{d}\bar{V} \tag{7}$$

$$\bar{V} = R^{2/3}S^{1/2}/n \tag{8}$$

where Q is the discharge of river. $\bar{d}$ and $\bar{V}$ denote average cross-sectional depth and velocity, respectively. W stands for the width of the cross-section. R is the hydraulic radius equivalent to the average depth of cross-section ($\bar{d}$). S represents the average energy gradient (channel slope), which can be extracted from digital elevation model or counter maps (Fonstad and Marcus, 2005). n is hydraulic resistance, which can be determined for mountain streams according to the following equation (Jarrett, 1984; Fonstad and Marcus, 2005):

$$n = 0.32S^{0.38}R^{-0.16} \tag{9}$$

By combining Eqs. 7, 8, and 9, $\bar{d}$ can be estimated for a given cross-section based on the river discharge (Q), width measurement from image, and slope measurements from topographic maps/data:

$$\bar{d} = (Q/3.12WS^{0.12})^{0.55} \tag{10}$$

In addition, HAB model approximates the maximum depth of each cross-section (d_{max}) based on Robison and Beschta's (1989) assumption:

$$d_{max} = 2\bar{d} \tag{11}$$

We have estimated $\bar{d}$ and d_{max} for a number of cross-sections along the Sarca River in order to assess the depth estimates from the proposed MODPA compared to other techniques. The HAAB provided an additional means of accuracy assessment, which allowed us to assess the bathymetry methods ubiquitously along the channel and independent from in-situ depths. Note that Q is the only field information required for this assessment approach, which was available from the gaging station in the study area.

5- Datasets

The effectiveness of MODPA compared to the Lyzenga model and OBRA was examined by performing a wide range of analyses on three independent datasets: (1) Spectroscopic experiments were performed at a hydraulic laboratory to acquire measurements of water depth and reflectance under controlled conditions. As substrate variability would be the key challenge for bathymetry retrieval in shallow and clearly flowing streams, robustness of the models was examined through experiments with two different bottom types (Section 5-1); (2) Simulated spectra were used to test the robustness of bathymetry models by isolating the effect of IOPs and also to evaluate their performance under optically complex conditions (Section 5-2); (3) A WV-2 image was used to map the bathymetry of the Sarca River from space considering both top of atmosphere (TOA) and AComp reflectances. A field survey was performed to collect in-situ depths for calibration and validation of models (Section 5-3). To perform consistent analyses, the spectral reflectances from different sources were convolved with the spectral response functions of the WV-2 and GeoEye sensors. The band designations of sensors are given in Table 1.

Table 1. Spectral band specifications for GeoEye and WV-2 sensors (DigitalGlobe, 2013).

GeoEye			**WV-2**		
Band	Center wavelength (nm)	Bandwidth (nm)	Band	Center wavelength (nm)	Bandwidth (nm)
Blue (B)	484	76	Coastal-Blue (CB)	427	62
Green (G)	547	81	Blue (B)	478	73
Red (R)	676	42	Green (G)	546	80
NIR	851	156	Yellow (Y)	608	48
			Red (R)	659	70
			Red Edge (RE)	724	50
			NIR1	833	136
			NIR2	949	187

5-1- Laboratory Experiments

A set of spectral reflectances was collected in an indoor hydraulic laboratory to test bathymetry models under controlled conditions of illumination, water level, IOPs, and bottom properties. These experiments are, to the best of our knowledge, the first to integrate spectroscopic and hydraulic facilities in an indoor laboratory, although similar experiments have previously been carried out by Legleiter and Overstreet (2014) in an outdoor environment. Two water flumes with different bottom properties were used to examine depth retrieval from spectral measurements (Fig. 1). Flume-1 was an 18 m long, 1 m wide and 0.7 m high channel with a layer of uniform fine sand on the bottom. Flume-2 was a 6 m long, 0.4 m wide, and up to 0.4 m deep with a semi-natural substrate consisting of natural sands combined with larger (3 cm diameter) ball-shape gravels with plastic material. Suspended sediment was considered as the main parameter defining the water column optical properties due to the fact that sediment load is the primary control on the IOPs of clear rivers (Legleiter and Overstreet, 2012; Legleiter et al., 2016). SSC was about 2 g/m^3 whereas the variation of this parameter was negligible between two flumes.

The channels were equipped with a flowmeter to measure the discharge and an adjustable tailgate weir was located at the end of the flume to control the water level and ensure a uniform flow condition. Experiments were focused on an area in the longitudinal and cross-sectional middle of each channel to ensure a well-developed flow and also to mitigate as much as possible the reflections and shadows from the flume sidewalls. Moreover, two sides of the smaller flume (flume-2) were covered with a low-reflective black material in the test area to minimize possible side reflections. The water depths were measured using a point-gage. The spectra were collected by installing over the test area a fiber optic jumper cable connected to an Analytical Spectral Devices (ASD) HandHeld2 spectroradiometer that allowed measurement of reflectance in the 325–1075 nm spectral range with 1 nm spectral resolution. Unstable lighting conditions were eliminated by covering the experiment area on flume-1 while flume-2 was located in a darkroom. A standard ASD illuminator was used to produce highly stable light across the full spectral range (350 – 2500 nm), which entirely covers the above mentioned operation range of the spectroradiometer. Spectra for a range of depths were collected from the two flumes by changing the water level in one cm increments. For each flow condition, three spectra were recorded as the average of

25 individual samples. Dark current and white reference measurements were taken and updated for each spectral recording in order to convert the raw spectra into reflectance.

Fig. 1. Spectroscopic experiments in a range of water depths on (a) flume-1with a sand bed and (b) flume-2 with a gravel bed composed of semi-natural material.

5-2- Radiative Transfer Simulations

Radiative transfer simulations have been used previously to examine the accuracy of OBRA by isolating the effects of substrate type and SSC in shallow rivers (Legleiter et al., 2009; Legleiter and Roberts, 2009). We performed simulations using the Hydrolight radiative transfer model (Mobley and Sundman, 2008) to examine the proposed MODPA by isolating the effect of IOPs by manipulating Chl-a, SSC, and CDOM. Long-term measurements of water quality parameters in Italian alpine rivers reported by the Trento Environment Protection Provincial Agency (Giardino et al., 2007) were used to define the range of IOPs used in the simulations. The relatively wide range of IOPs assumed for radiative transfer simulations permitted the evaluation of bathymetric models not only in normal conditions of the Sarca River but also in extreme conditions of IOPs (relatively turbid waters). This broader range of IOPs and water depth for the simulated data can thus be used to assess the feasibility of extending our approach to other rivers with similar optical properties.

The effect of each IOP was isolated by considering constant values for the other IOPs (Table 2). Note that dolomite, which is dominant bottom type in the Sarca River study region, was considered for these simulations and the water depth varied from 2 cm to 2 m in 2 cm increments. For each experiment, 300 spectral reflectances were simulated for which half of the data, selected at random, were used for calibration of the models and the remaining data reserved for validation. The CDOM absorption at 440 nm, a_{CDOM} (440), was chosen to quantify the influence of this constituent on this IOP (Kirk, 1996).

Table 2. The range of IOPs considered for Hydrolight simulations. The effect of variations in each of IOPs was isolated by considering constant values for other IOPs.

Isolated IOP (variable)	Other IOPs (constant)
Chl-a = [1, 3, 5] mg/m^3	SSC= 3 g/m^3, a_{CDOM}(440)= 0.22 m^{-1}
SSC= [0, 3, 6] g/m^3	Chl-a= 3 mg/m^3, a_{CDOM}(440)= 0.22 m^{-1}
a_{CDOM}(440)= [0.07, 0.22, 0.36] m^{-1}	Chl-a= 3 mg/m^3, SSC= 3 g/m^3

In addition, an optically-complex condition was also considered to explore the effectiveness of bathymetry models by treating all of the IOPs and also the bed type as variable parameters. Three different bottom types (dark sediment, macrophyte, and dolomite) were considered in the same range of IOPs and water depths of previous simulations, resulting in 8100 individual spectra. Spectral reflectances of the three bottom types are shown in Fig. 2 which are characteristics of both bright and dark substrates.

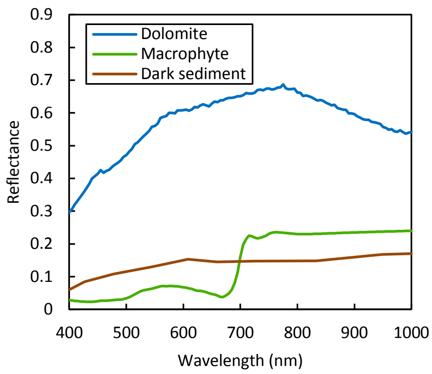

Fig. 2. Spectral reflectances of bottom types used in radiative transfer simulations.

5-3- WV-2 Image and In-Situ Measurements

An 8-band WV-2 image and its spectral convolution with GeoEye's band passes (Table 1), were used to map the bathymetry of the Sarca River. The Sarca is a mountain-piedmont gravel-bed river flowing from the Adamello glaciers down to Lake Garda in northeast Italy. It is a shallow (depth <1 m), narrow (mean width < 30 m), and clearly flowing stream which is regulated by an upstream dam that maintains a very consistent water level with a minimal sediment load during a long period of several years. A WV-2 image was used for which both TOA and AComp (Pacifici et al., 2014) reflectances were available. AComp provides an estimate of aerosol optical depth and water vapor independently in each pixel and applies the atmospheric correction by accounting for adjacency effects (Pacifici, 2016; DigitalGlobe, 2016). In addition, we spectrally convolved the WV-2 image with the spectral response function of the GeoEye sensor to gain more insight into the effectiveness of the additional spectral bands of the WV-2 imagery over traditional 4-band (RGB-NIR) HRSI like GeoEye for mapping river bathymetry.

The field survey was carried out in three reaches along the river to gather depth samples as representative as possible for different environmental conditions (depth, bottom type, etc.). The in-situ depths were recorded with precise coordinates using RTK GPS along cross-sections with about one to two meter distances (Fig. 3). An ordinary block kriging was used to interpolate the measured depths at the pixel scale to enable a pixel-to-pixel comparison of in-situ depths with the image-derived estimates (Legleiter and Overstreet, 2012).

Fig. 3. In-situ measurements of water depths in **(a)** three reaches of the Sarca River, using **(b)** a RTK GPS **(c)** at dense points along cross-sections. The location of river is highlighted in northeast Italy.

6- Results

The bathymetry models were applied to spectroscopic data collected in the laboratory, synthetic data from radiative transfer modeling, and HRSI. Findings are presented and discussed in the following subsections.

6-1- Laboratory Experiments

The parameters of the bathymetric models were estimated using half of the observations over both flumes, selected at random, to gain insight into the robustness of the models with respect to substrate variations between the flumes. Fig. 4 represents the predicted vs. observed depths using WV-2 spectra for validation samples. For brevity, the match-ups between predicted and observed depths for the simple Lyzenga model that provided the lowest accuracies are dropped from all figures but the accuracy statistics are provided on bar charts.

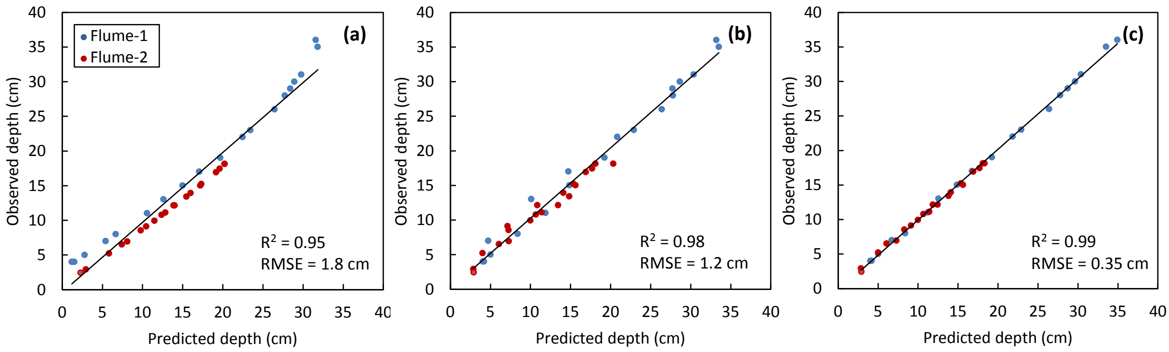

Fig. 4. Validation of depths derived from **(a)** OBRA, **(b)** multiple Lyzenga and **(c)** MODPA based on PLS regression using laboratory spectra convolved to WV-2 bands.

The OBRA matrices illustrated in Fig. 5 show the R^2 and RMSE of the ratio model for all possible combinations of spectral bands; the highest regression R^2 occurred for the ratio between the yellow and the red-edge bands (Y/RE).

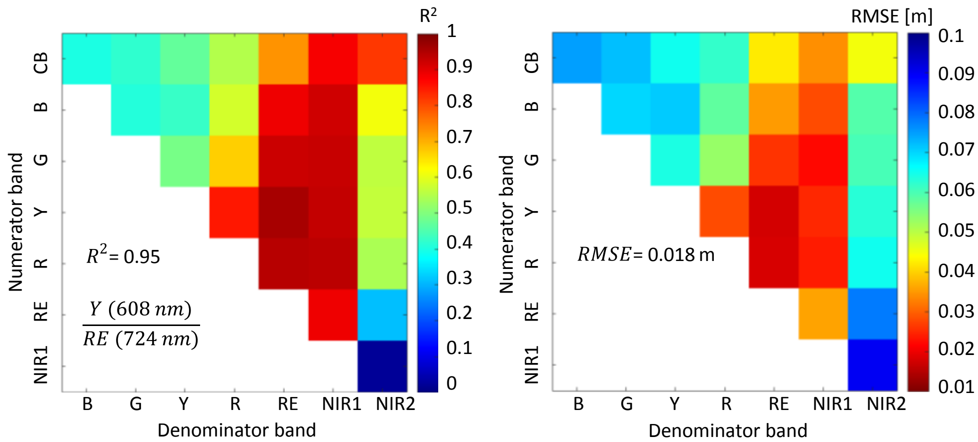

Fig. 5. OBRA of laboratory WV-2 spectra representing R^2 and RMSE of the ratio bathymetry model for all the possible combination of spectral bands.

As evident in Fig. 4, the retrievals from OBRA were sensitive to the substrate types of the two flumes. The relatively bright substrate in flume-1 has been confused with shallower depths while the darker bottom-type of the flume-2 led to overestimation of depths. The multiple Lyzenga model and MODPA were both robust with respect to substrate variability. However, the residuals from MODPA were about four times smaller than those of multiple Lyzenga (0.35 cm vs. 1.2 cm RMSEs).

The accuracy statistics of bathymetry models with and without intensity predictors are compared for the laboratory spectra convolved to both WV-2 and GeoEye bands in Fig. 6. The three different regression approaches (i.e., PLS, stepwise and PC) provided high accuracies for the proposed MODPA. However, MODPA based on PLS regression was slightly more accurate than the other two forms of regression. The optimal model, PLS-based MODPA, was composed of one Lyzenga predictor derived from the RE band and three ratio predictors derived from G/NIR1, Y/RE and R/RE ratios for the laboratory WV-2 spectra. The extra predictors improved the accuracies of bathymetry retrievals. The improvements were more pronounced for the spectra convolved to a lower number of bands (i.e., 4-band GeoEye), and we inferred that the enhanced spectral resolution of WV-2 led to more accurate depth retrievals than GeoEye.

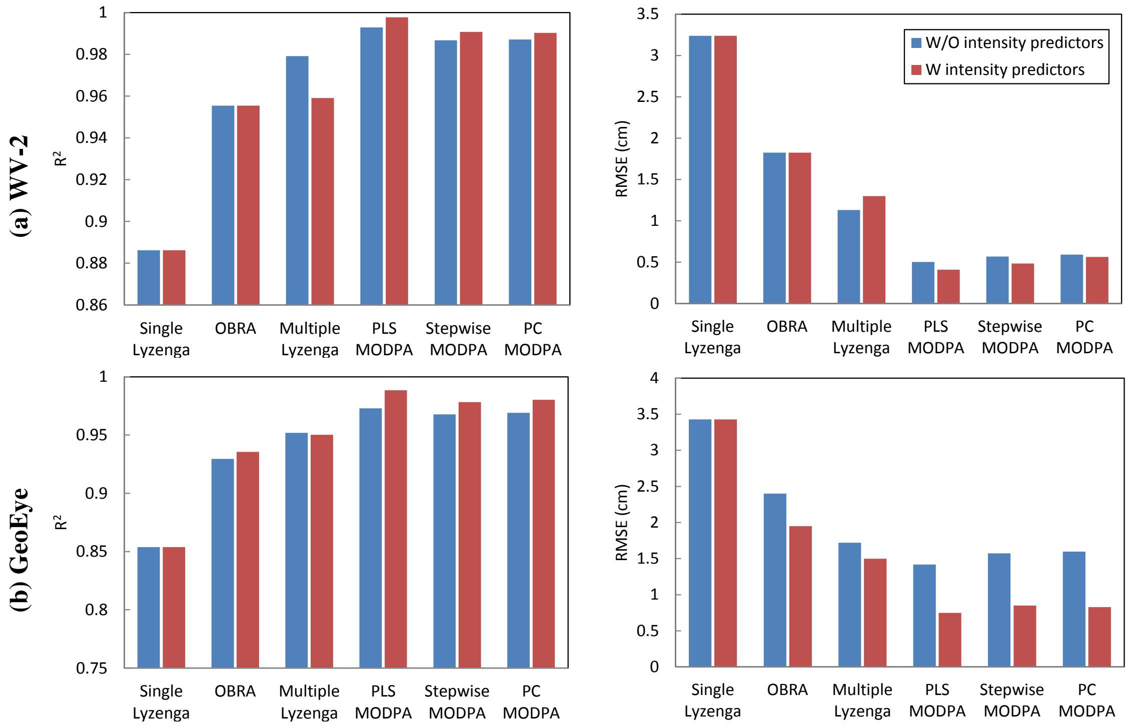

Fig. 6. Accuracy statistics (R^2 and RMSE) of bathymetry models with (W) and without (W/O) intensity predictors applied to laboratory spectra convolved to match **(a)** WV-2 and **(b)** GeoEye bands.

6-2- Synthetic Data Analysis

6-2-1- Isolating the Effect of IOPS

Fig. 7 illustrates the results of isolating the effect of variations in IOPs for waters with up to 2 m depth. The OBRA-based retrievals were sensitive to changes in concentrations of each IOP. According to Legleiter et al. (2009), the exponential relation between radiance and depth is subject to failure as depth increases. This is because IOPs, particularly as influenced by SSC, imply greater scattering in a thicker water column. As evident in Fig. 7, mismatches between the OBRA retrievals and known depths are more pronounced for the higher depths, particularly with high SSC. The multiple Lyzenga model and MODPA showed very good performance, but the residuals were smaller for the proposed MODPA.

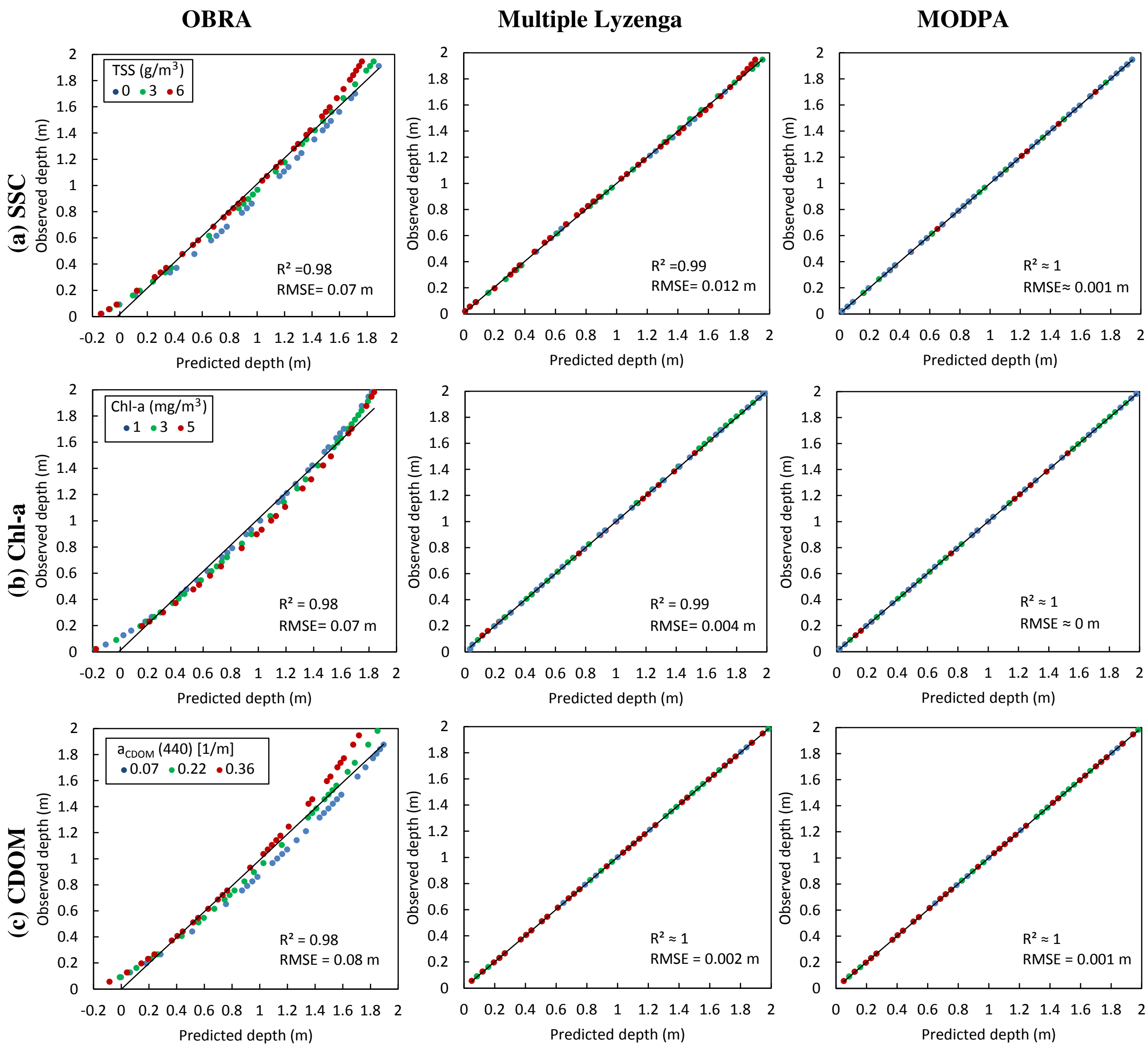

Fig. 7. Match-up validation of different bathymetry models by isolating the effect of IOPs including **(a)** SSC, **(b)** Chl-a, and **(c)** CDOM.

6-2-2- Optically-Complex Shallow Waters

In this testing strategy, we have assumed shallow waters with variable bottom-types and IOPs (see Section 5-2). MODPA led to the highest correlation with known depths (R^2 = 0.98 and RMSE= 6 cm without considering intensity predictors). Including the intensity predictors further enhanced depth retrieval using MODPA (RMSE= 3 cm). This demonstrated the effectiveness of intensity predictors for improving the robustness of bathymetry models in optically-complex waters. The match-up validations indicated significant improvement (i.e., 7 cm better RMSE) of depth retrieval using MODPA compared to the multiple Lyzenga model (Fig. 8).

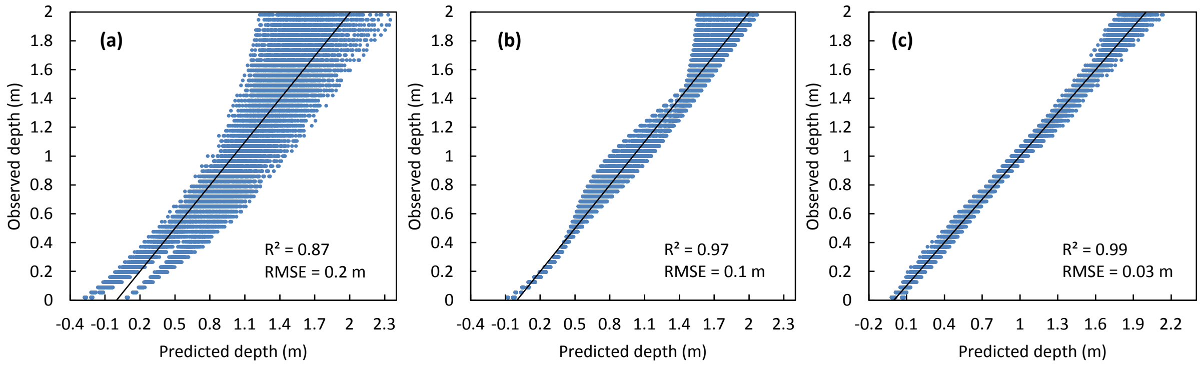

Fig. 8. Match-up validation of depth retrieval based on **(a)** OBRA, **(b)** Multiple Lyzenga and **(c)** MODPA with intensity predictors for the optically complex spectra with variable IOPs and bottom types.

We performed further analysis to understand if hyperspectral data could improve the performance of OBRA in the optically-complex testing scenario. Radiative transfer simulations with a spectral resolution of 10 nm were used to perform OBRA in the spectral range of 400 nm to 900 nm. As evident in Fig. 9, depth retrieval for the optimal pair of ratio bands has been improved compared to that of 8-band WV-2 data, but required very high spectral resolution (i.e., 50 bands in the range of 400 nm to 900 nm). However, the results are not comparable with MODPA (RMSE of 3 cm for MODPA vs. 15 cm for OBRA using hyperspectral data). This indicates that utilizing multiple predictors derived from a relatively low spectral resolution data (8-band WV-2) through MODPA is much more effective than when using a single predictor model like OBRA, even with high spectral resolution. Note that the wavelength position rather than the spectral resolution of hyperspectral data can also influence the performance of OBRA (Legleiter et al., 2009).

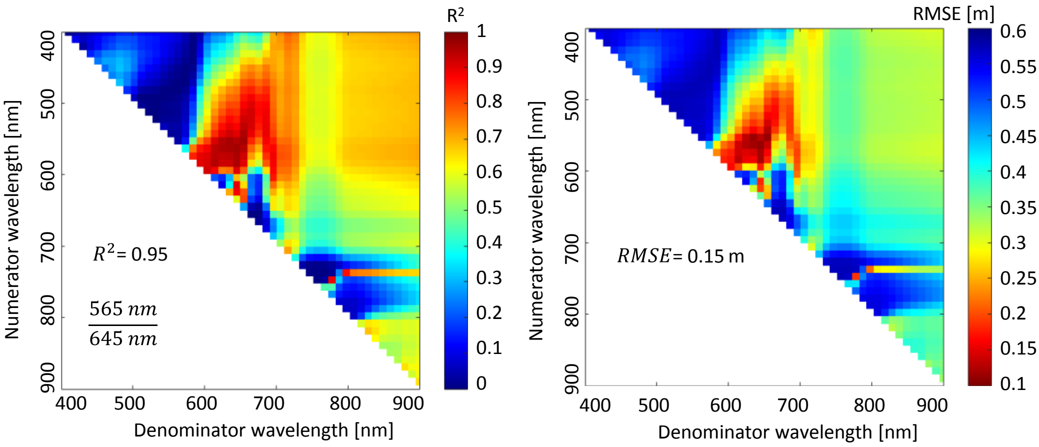

Fig. 9. OBRA of simulated spectra with 10 nm spectral resolution for the optically-complex testing scenario.

6-3- WV-2 Image Analysis

Atmospheric effects can make a significant contribution to the TOA radiance at short wavelengths (mainly visible bands) due to the low reflectivity of water bodies (Gordon, 1990; Pahlevan et al., 2017). Fig. 10 compares the AComp reflectances (i.e., surface reflectances) with TOA reflectances for WV-2 image pixels from a range of water depths along the Sarca River. The image-derived reflectances were averaged for all pixels with a given depth known from the field survey. As evident in Fig. 10, atmospheric effects were significant at short wavelengths dominated by Rayleigh scattering (Gordon 1990; Pahlevan et al., 2017). AComp and TOA reflectances of the WV-2 image were then supplied to the bathymetry models to investigate robustness of the models with respect to atmospheric effects.

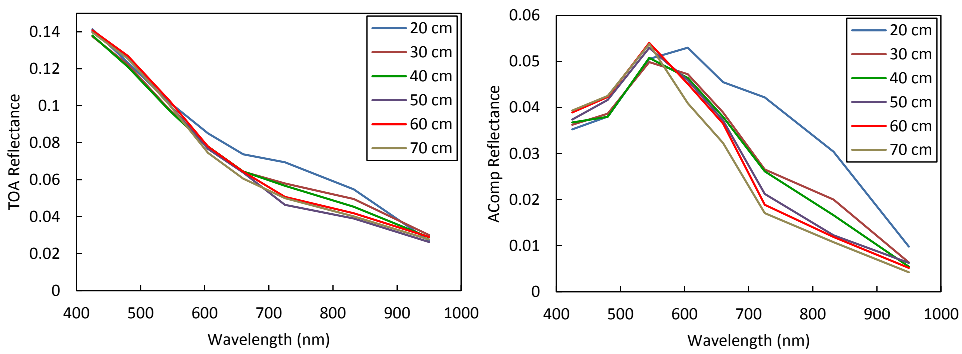

Fig. 10. Comparison of TOA and AComp reflectances of WV-2 image in a range of water depths along the Sarca River.

As first validation approach, one half of the data was reserved for calibration of models and the remaining half for accuracy assessment. Note that substrate compositions such as algae cover and also water column constituents can vary over distances of less than a meter in small rivers such as our case study (Fonstad and Marcus, 2005), which can significantly complicate the depth retrieval. Fig. 11 illustrates the validation of bathymetry models based on TOA reflectances from the WV-2 image; MODPA provided the highest accuracy. The residual plots indicate absolute errors of up to 0.4 m for OBRA and multiple Lyzenga methods, whereas MODPA provided depth estimates with residuals smaller than 0.2 m.

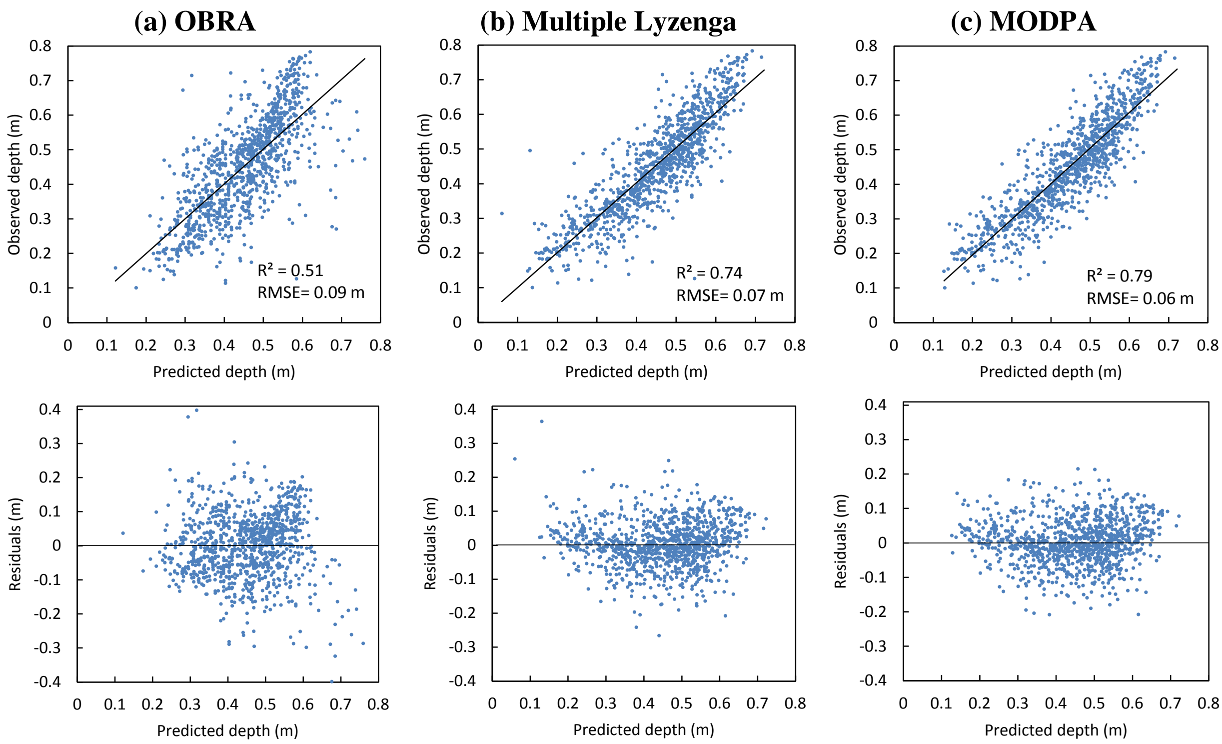

Fig. 11. Validation of depth retrieval from TOA reflectances of WV-2 image based on **(a)** OBRA, **(b)** Multiple Lyzenga and **(c)** MODPA using PLS regression.

Fig. 12 shows the OBRA matrix obtained from TOA reflectances of WV-2 image for which G/R ratio yielded the highest observed vs. predicted R^2 (0.51) with an RMSE of 9 cm. The matrix indicates that band ratios with a B or G numerator and a RE or NIR1 denominator as well as Y/RE ratio also provided comparable results with the optimal band ratio (i.e., G/R). This demonstrates the potential of long wavelengths across the near-infrared spectrum in retrieving the bathymetry in shallow and clear waters as long as the water column depth is not too great and the IOPs do not dictate complete absorption or scattering of the signal.

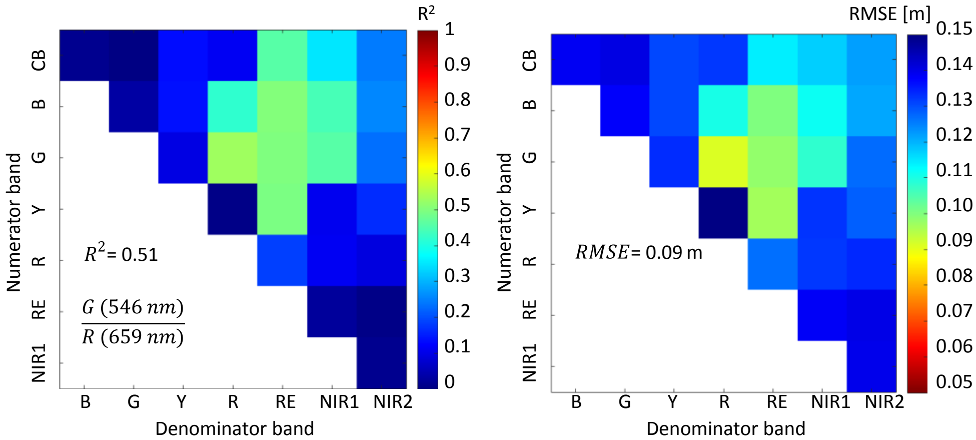

Fig. 12. OBRA using TOA reflectances of WV-2 image representing R^2 and RMSE of the ratio model for all the possible combination of spectral bands.

Fig. 13 shows the retrieved bathymetry maps from TOA reflectances compared to in-situ depths along three reaches of the Sarca River.

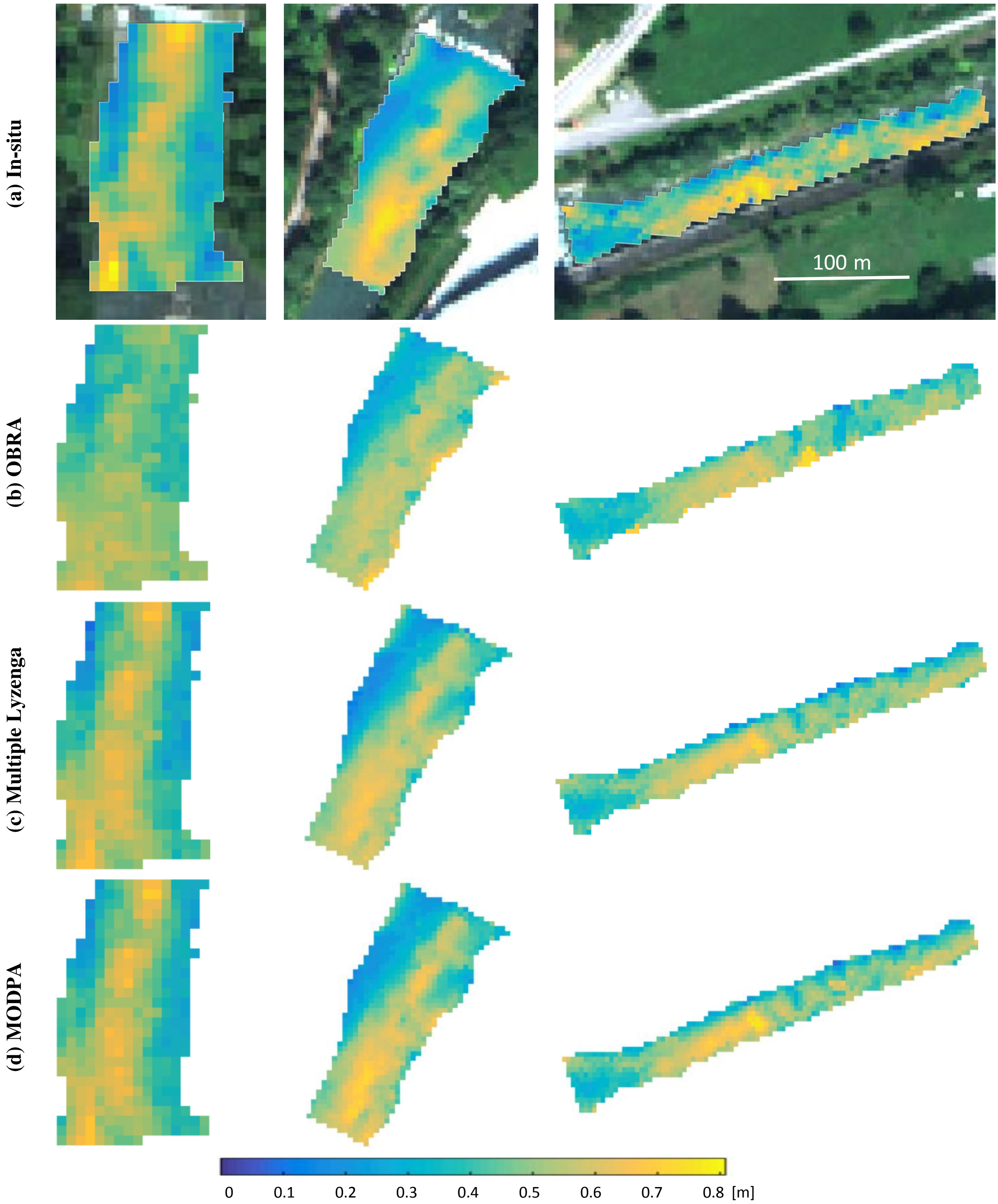

Fig. 13. Comparison of **(a)** in-situ depths with bathymetry maps derived from **(b)** OBRA, **(c)** Multiple Lyzenga model and **(d)** MODPA.

The accuracy statistics of bathymetry models with and without intensity predictors are compared for the WV-2 image and its convolution to GeoEye bands in Fig. 14. In addition, AComp reflectances were examined relative to the TOA reflectances using the WV-2 image. In general, the AComp reflectances yielded higher accuracies than TOA reflectances. However, the accuracy enhancement was more pronounced for OBRA, whereas MODPA was less affected by atmospheric effects. Again, the three approaches for selection of optimal predictors provided comparable results, but the PLS regression was slightly more accurate than the others. This model was composed of three Lyzenga predictors derived from CB, G and RE bands and two ratio predictors derived from G/R and G/NIR1 using the WV-2 image.

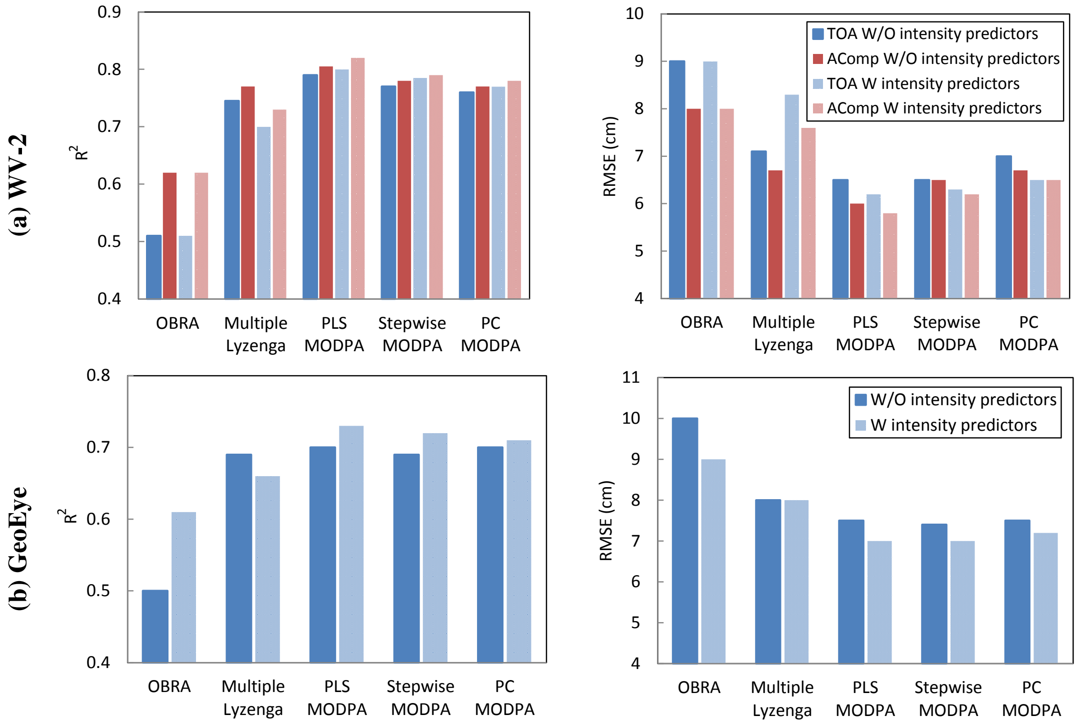

Fig. 14. Accuracy statistics (R^2 and RMSE) of bathymetry models with (W) and without (W/O) intensity predictors applied on **(a)** WV-2 and **(b)** GeoEye images. The comparison also performed for the TOA and AComp reflectances of the WV-2 image.

As can be inferred from Fig. 14, the intensity predictors in general led to an increase of R^2 for all the models except for the Lyzenga's multiple regression model. This is mainly because making use of all the Lyzenga predictors derived from original bands and intensity components induces the overfitting problem as well as degradation of predictive power due to the presence of irrelevant predictors. As an interesting point, intensity predictors for the GeoEye image remarkably increased the accuracy of OBRA (about 0.1 enhancement of R^2). This is shown in Fig. 15 where the optimal ratio model has been derived from intensity (I) bands.

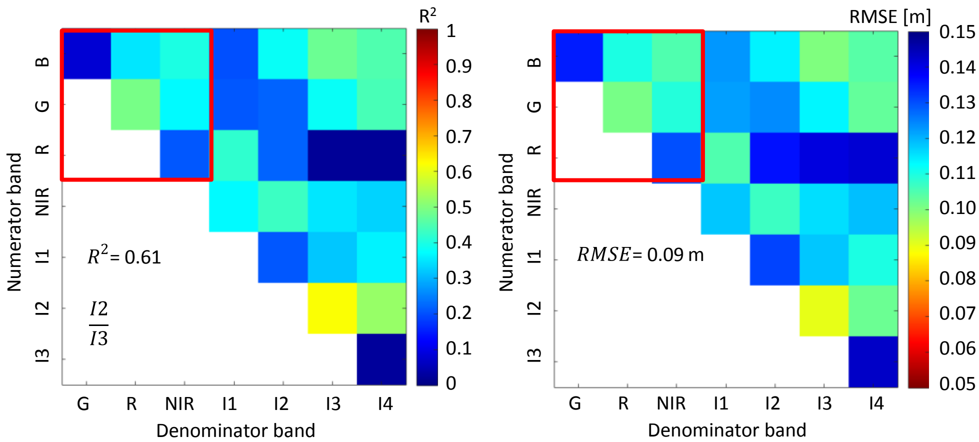

Fig. 15. OBRA of GeoEye image where the OBRA matrix derived from the original image bands (RGB color space) is highlighted with a red box. The optimal band ratio model was derived from intensity (I) predictors.

Fig. 16 compares the bathymetry retrieved from the WV-2 image with in-situ observations along a few randomly selected cross-sections.

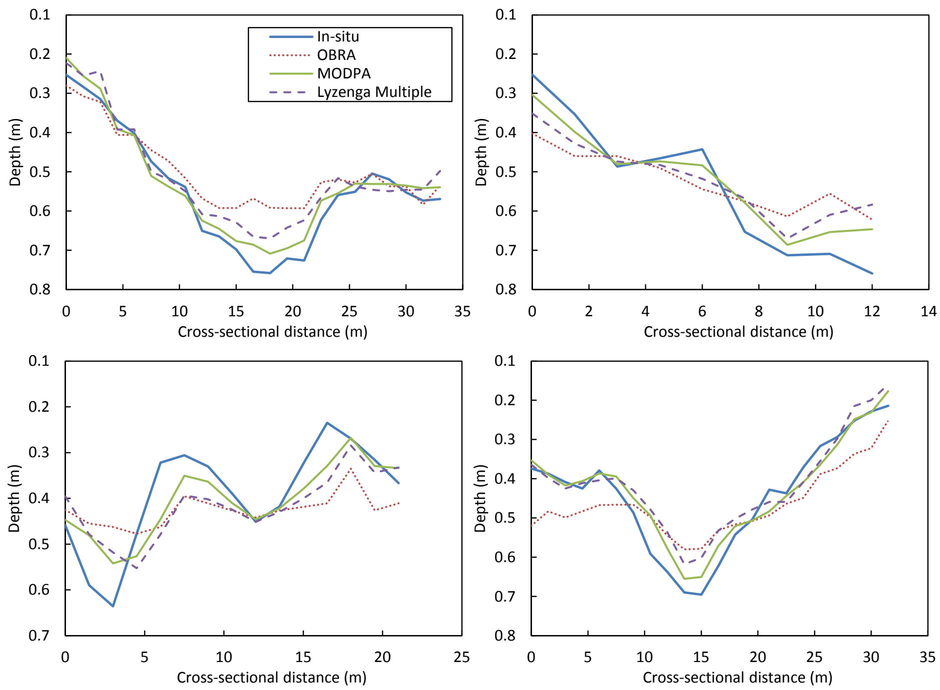

Fig. 16. Comparison of in-situ depths along cross-sections of the Sarca River with bathymetry retrieval from different models considering intensity predictors using WV-2 image.

We performed an additional analysis to investigate the performance of bathymetry models with spatially distant samples for calibration and validation. In this context, the two distal in-situ reaches were used for calibration and the middle one for validation. Fig. 17 shows the depth maps and the accuracy statistics derived from bathymetric models for the middle reach of the Sarca River. The results demonstrated the increased validity and robustness of MODPA compared to other methods.

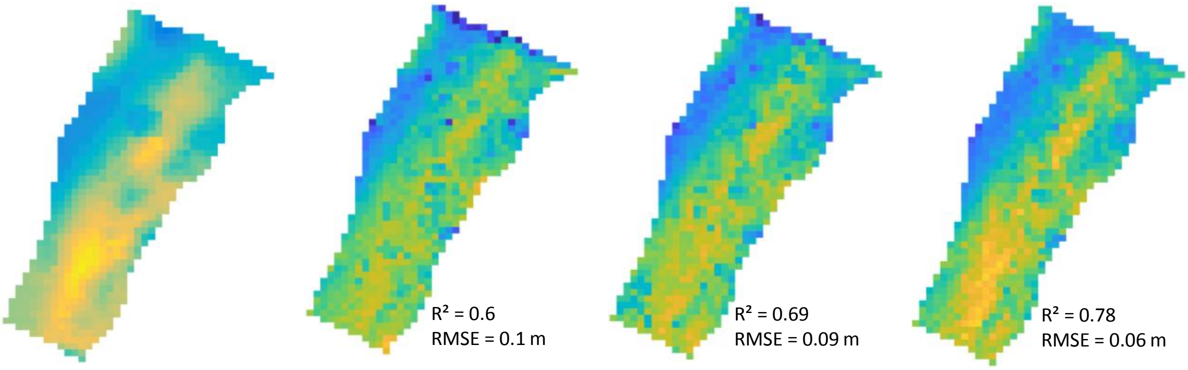

(a) In-situ (b) OBRA (c) Multiple Lyzenga (d) MODPA

Fig. 17. Depth maps estimated for the middle reach of the Sarca River by calibrating the bathymetry models with two distal in-situ reaches.

In addition, we estimated mean and maximum depths for 50 cross-sections regularly spaced along a 3 km reach of the Sarca River to perform HAAB (Eqs. 10 and 11). In this regard, the discharge of the river was available from gage records (Q = 4.6 m^3/s). Regional slopes of the channel were estimated from an available LiDAR-derived digital surface model ($0.01 < S < 0.003$) and cross-sectional widths (W) were measured on the image. The depth estimates based on HAAB allowed us to perform an independent analysis on the efficacy of bathymetry models in reaches where no in-situ measurement was available. The proposed MODPA resulted in a more accurate depth estimates compared to OBRA and multiple Lyzenga models. MODPA-based depth estimates indicate enhancement of R^2 on the order of 0.22 and 0.11 with RMSE improvement of 0.06 m and 0.05 m compared to OBRA and multiple Lyzenga models, respectively (Fig. 18).

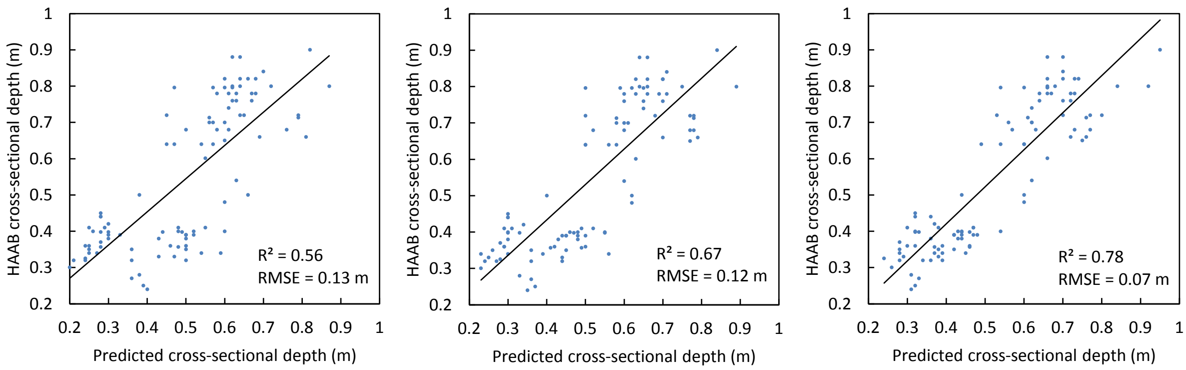

Fig. 18. Mean and maximum cross-sectional depths from HAAB compared with depth retrievals from WV-2 image based on (a) OBRA, (b) Multiple Lyzenga and (c) MODPA using PLS regression.

The bathymetric map derived from the WV-2 image for a 5 km-long reach using the proposed MODPA based on PLS regression is shown in Fig. 19. In addition to the quantitative assessment performed on independent check points described above, visual inspection also supports the realism of the map, with the pool-to-pool spacing across the reach corresponding to the theoretically established 5-7 channel widths (Montgomery et al., 1995).

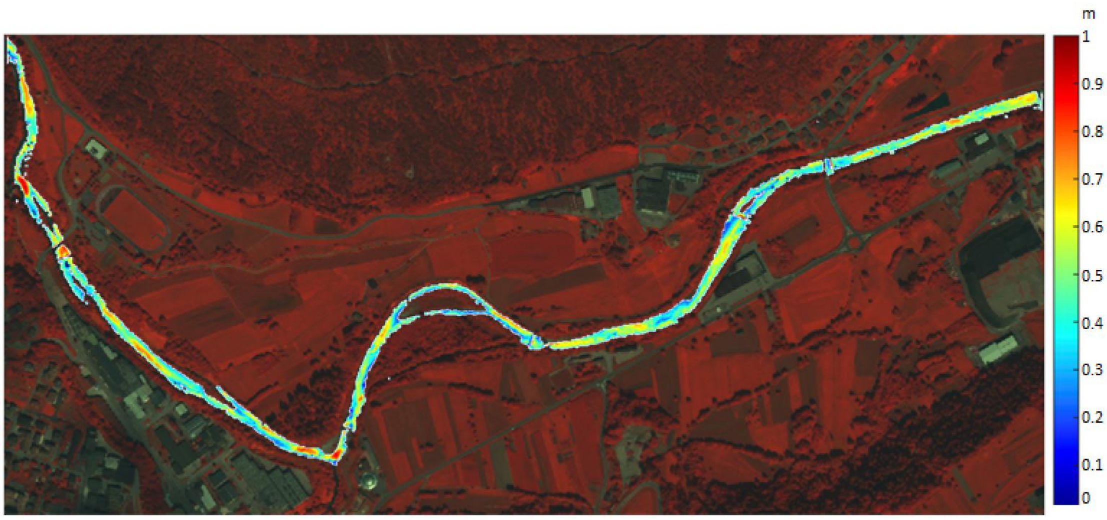

Fig. 19. Bathymetry map derived from the proposed MODPA based on PLS regression using WV-2 image.

7- Discussion

Lyzenga's single predictor demonstrated to be very sensitive to variations in substrate type and IOPs. Although this predictor individually failed in providing depth information, it might have potential for classifying riverbed compositions. The OBRA also failed to provide satisfactory, robust depth retrieval with respect to substrate and IOPs variability. Despite identification of the optimal pair of bands for the ratio model, OBRA is a single predictor model and most likely neglects other explanatory variables even when using very high spectral resolution data. Multiple Lyzenga predictors enhanced the robustness of the model with respect to optically complicating factors in riverine environments. However, this model does not account for any process to select optimal predictors and might lead to overfitting problems that could degrade prediction accuracies due to the risk of correlated and redundant predictors. This problem would become even more significant when using high-dimensional (hyperspectral) imagery and also when considering additional candidate predictors such as intensity components used in this study. The performance of the multiple Lyzenga model on WV-2 data was degraded by including the intensity predictors. This finding highlights the significance of using MODPA to identify optimal predictors, among all the candidate predictors, including the intensity components. Moreover, intensity predictors were most significant when there were more complexities in the data (Fig. 8). This is reasonable as the main rationale for adding new predictors is to deal with complex data and enhance robustness with respect to all undesirable variations. As OBRA and proposed MODPA identify the optimal predictor/s, they yielded improved results when using intensity predictors. More specifically, the single predictor of OBRA for the GeoEye image was a combination of intensity predictors. This result shows the effectiveness of extra predictors such as intensity components for bathymetry mapping from imagery with low spectral resolution. The results of bathymetry models applied to simulated spectra further suggested the robustness of MODPA with respect to changes in IOPs (as influenced by SSC, Chl-a and CDOM) and also in optically-complex rivers where all the IOPs as well the bottom types were variable. The intensity predictors improved the results of MODPA in the testing scenario associated with the simulated optically-complex rivers (3 cm improvement of RMSE for depths up to 2 m). Moreover, the range of predicted depths for MODPA was more in agreement with the known depths whereas other methods were hindered by estimation of some negative depths in the optically-complex testing scenario (see Fig. 8).

The enhanced spectral resolution of WV-2 showed benefits for mapping the bathymetry of shallow rivers. For instance, the long-wavelength bands including RE and NIR1 proved to be useful as Lyzenga predictors or as the denominator of ratio-based predictors. This is mainly because light in shallow and clear rivers is not fully attenuated even for long/highly-absorbing wavelengths. On the other hand, short-wavelength bands (e.g. B, CB, G and Y) performed as appropriate numerator bands for ratio predictors. In summary, the WV-2 sensor provided a wealth of options for selecting either Lyzenga or ratio predictors and led to higher accuracies than when using 4-band GeoEye data (e.g., improvements of R^2 and RMSE respectively on the order of 9% and 1 cm using TOA reflectances without intensity predictors). Comparing the TOA and AComp reflectances over a range of field-measured depths showed reasonable correction of atmospheric effects (e.g., appropriate removal of Rayleigh scattering over short wavelengths). AComp reflectances yielded higher accuracies than TOA data, with a more pronounced difference for OBRA (improvements of R^2 and RMSE on the order of 11% and 1 cm, respectively). However, multiple-predictor models, particularly MODPA, showed robust bathymetry retrievals with respect to atmospheric effects. MODPA provided promising results and improvements for bathymetry retrieval in the Sarca River based on a WV-2 image. The best result was derived from MODPA based on PLS regression using AComp reflectances where R^2 and RMSE were estimated as 0.82 and 5.8 cm, respectively. Although the three investigated regression methods provided very comparable results, the PLS-based regression showed slightly more accurate results. The imaged-derived bathymetry of the Sarca River validated based on two different sampling strategies for calibration of the models and also by comparing with the cross-sectional depth estimates from basic models of river hydraulics (i.e., HAAB).

8- Conclusions and Future Work

The thinner and less complex water columns of shallow and clearly flowing rivers permit the bottom component of radiance to dominate the signal reaching the sensor. Although this radiance component is desired for bathymetry retrieval, it is affected not only by water depth but also by substrate type/composition and indirectly by water column properties (IOPs). Moreover, other factors such as highly variable roughness of the water surface, variable IOPs, and atmospheric effects can complicate depth retrieval in riverine environments. Therefore, development of methods robust to all these variations is essential in order to retrieve consistent bathymetric data over large spatial and temporal extents using optical imagery. This research introduced MODPA to take advantage of both Lyzenga and ratio predictors and also to integrate extra predictors obtained from the intensity component of the HSI color space. In this regard, all the possible Lyzenga and ratio predictors derived from the original image as well as the intensity components were considered as candidate predictors. A set of optimal predictors were then selected based on one of PLS, PC or stepwise regressions.

The proposed MODPA outperformed widely-used OBRA and multiple Lyzenga methods through three independent analyses using laboratory spectra, radiative transfer model simulations, and satellite data. The significance of MODPA was demonstrated in optically-complex waters by providing robust retrievals with respect to variations in substrate type, IOPs, water surface roughness, and atmospheric effects. Additional predictors (e.g. spectral water indices) could be included in the MODPA particularly for low spectral resolution imagery or for studies on optically-complex waters, which will be the subject of future investigations. The radiative transfer simulations were representative of a wide range of IOPs in the study region, including turbid waters. However, more research should be dedicated to study turbid rivers to further explore the potential of MODPA. The first tests on DigitalGlobe AComp indicated the effectiveness of this product for mapping the bathymetry of shallow and clearly flowing rivers. However, more studies should be dedicated to comprehensively analyze the quality of AComp product for remote sensing of inland waters.

Note that the key for empirical depth retrieval methods is to have a sufficient number of samples available for calibration to allow the regression model to capture the variability and complexity of the data. In the cases with limited number of in-situ samples, cross-validation approaches (Martens and Dardenne, 1998) and also the hydraulic-based approach considered in this study (i.e., HAAB) would be beneficial to perform the calibration and validation of bathymetric models. Moreover, HAAB allows to examine the reliability of depth retrievals in the reaches without available in-situ depths.

This research demonstrated the effectiveness of spectroscopic experiments in an indoor environment of a hydraulic laboratory to study the bathymetry of very shallow waters considering variable bottom types. Experiments of this kind can be extended to study other attributes of fluvial systems such as flow velocity and water quality indicators. The proposed MODPA was demonstrated to be an efficient technique for mapping river bathymetry. However, application of this technique is restricted neither to riverine environments nor to a specific optical sensor. MODPA has the potential for application to any multi/hyper-spectral image over optically shallow inland or coastal waters. The sensor and platform type can be defined based on requirements of the case study, such as the spatial resolution. Further assessment of MODPA using freely-available Sentinel-3, Sentinel-2, and Landsat-8 imagery would be interesting in various coastal/inland applications.

Acknowledgments

This work was carried out within the SMART Joint Doctorate (Science for the MAnagement of Rivers and their Tidal systems) funded with the support of the Erasmus Mundus programme of the European Union. The authors acknowledge the imagery grant awarded by DigitalGlobe Foundation for providing theWV-2 imagery. We acknowledge the Alexander Goetz instrument support program of ASD Inc. for awarding us a short-term usage of HandHeld2 spectroradiometer. The authors are grateful to Prof. Aronne Armanini, Prof. Maurizio Righetti and Prof. Guido Zolezzi for giving access to the hydraulic laboratory at the University of Trento and their supports during the experiments. We would like to greatly appreciate Dr. Nima Pahlevan at NASA Goddard Space Flight Center (GSFC) for providing the Hydrolight simulations. We also highly appreciate constructive comments from Dr. Patrice Carbonneau and two other anonymous reviewers, which improved the manuscript.

References

Abdi, H., 2003. Partial Least Square Regression (PLS Regression). In Encyclopedia of Social Science Research Methods; SAGE: Thousand Oaks, CA, USA, pp. 792–795.

Bramante, J.F., Raju, D.K., and Sin, T.M., 2013. Multispectral derivation of bathymetry in Singapore's shallow, turbid waters, *International Journal of Remote Sensing*, 34:6, 2070-2088.

Brando , V.E., Anstee, J.M., Wettle, M., Dekker, A.G., Phinn, S.R., Roelfsem, C., 2009. A physics based retrieval and quality assessment of bathymetry from suboptimal hyperspectral data. *Remote Sensing of Environment*, 113, 755–770.

Bryant, R.G., Gilvear, D.J., 1999. Quantifying geomorphic and riparian land cover changes either side of a large flood event using airborne remote sensing: River Tay, Scotland. *Geomorphology*, 29 (3/4): 307–321.

Carbonneau, P., Fonstad, M.A., Marcus, W.A., Dugdale, S.J., 2012. Making riverscapes real. *Geomorphology*, 137 (1), 74–86.

Carbonneau, P.E., Lane, S.N., Bergeron, N., 2006. Feature based image processing methods applied to bathymetric measurements from airborne remote sensing in fluvial environments. *Earth Surface Processes and Landforms*, 31, 1413–1423.

Carbonneau, P.E., Lane, S.N., Bergeron, N.E., 2004. Catchment-scale mapping of surface grain size in gravel bed rivers using airborne digital imagery, *Water Resources Research*, 40 (7).

Carper, W.J., T. M. Lillesand, and R. W. Kiefer, 1990. The Use of Intensity-Hue-Saturation Transformations for Merging SPOT Panchromatic and Multispectral Image Data, Photogrammetric *Engineering & Remote Sensing*, 56(4):459-467.

Dekker, A.G., Phinn, S.R., Anstee, J., Bissett, P., Brando, V.E., Casey, B., Fearns, P., Hedley, J., Klonowski, W., Lee, Z.P., Lynch, M., Lyons, M., Mobley, C.,Roelfsema, C., 2011.Intercomparison of shallow water bathymetry, hydro-optics, and benthos mapping techniques in Australian and Caribbean coastal environments. *Limnol. Oceanogr. Methods*, 9, 396–425.

Dierssen, HM, Zimmerman, RC, Leathers, RA, Downes, TV, Davis, CO. 2003. Ocean color remote sensing of seagrass and bathymetry in the Bahamas Banks by high-resolution airborne imagery. *Limnology and Oceanography*, 48: 444–455.

Dietrich, J.T., 2017. Bathymetric Structure-from-Motion: extracting shallow stream bathymetry from multi-view stereo photogrammetry. *Earth Surface Processes and Landforms*, 42: 355–364.

DigitalGlobe, 2013. spectral Response for DigitalGlobe Earth Imaging Instruments. Available at: https://dg-cms-uploads-production.s3.amazonaws.com/uploads/document/file/105/DigitalGlobe_Spectral_Response_1.pdf, Last access on 14/6/2018.

DigitalGlobe, 2016. DigitalGlobe Atmospheric Compensation. Available online: http://digitalglobe-marketing.s3.amazonaws.com/files/documents/AComp_WP_ACOMP.pdf (accessed on 14 June 2018).

Durand, M., Gleason, C. J., Garambois, P. A.,. Bjerklie, D., Smith, L. C.,Roux, H.,Rodriguez, E., Bates, P.D.,Pavelsky, T.M., Monnier, J.,Chen, X., Di Baldassarre,G., Fiset, J.M.,Flipo, N.,Frasson, R.P.d.M., Fulton, J., Goutal, N., Hossain, F., Humphries, E., Minear, J.T., Mukolwe, M.M.,Neal, J.C.,Ricci, S.,Sanders, B.F., Schumann,G., Schubert, J. E., andVilmin, L.,2016, An intercomparison of remote sensing river discharge estimation algorithms from measurements of river height, width, and slope, *Water Resources Research*, 52, 4527–4549.

Flener, C., 2013. Estimating deep water radiance in shallow water: adapting optical bathymetry modeling to shallow river environments. *Boreal Environment Research*. 18: 488–502.

Flener, C., Lotsari, E., Alho, P., Käyhkö, J., 2012. Comparison of empirical and theoretical remote sensing based bathymetry models in river environments. *River Research and Applications*, 28 (1), 118-133.

Flener,C., Vaaja, M.,Jaakkola, A, Krooks, A., Kaartinen, H., Kukko, A., Kasvi, E., Hyyppä, H.,Hyyppä, J., and Alho, P., 2013, Seamless Mapping of River Channels at High Resolution Using Mobile LiDAR and UAV-Photography. *Remote Sensing*, 5, 6382-6407.

Fonstad, M. A., and Marcus, W. A ., 2005. Remote sensing of stream depths with hydraulically assisted bathymetry (HAB) models. Geomorphology, 72, pp. 320–339.

Fryer, J.G., 1983. A simple system for photogrammetric mapping in shallow water, Photogrammetric Record, 11(62):203-208.

Giardino, C., Brando, V.E., Dekker, A.G., Strömbeck, N., Candiani, G., 2007. Assessment of water quality in Lake Garda (Italy) using Hyperion. *Remote Sensing of Environment*, 109 (2), pp. 183-195.

Gitelson, A.A. and Kondratyev, K.Y., 1991, Optical models of mesotrophic and eutrophic water bodies. *International Journal of Remote Sensing*, 12, pp. 373–385.

Gordon, H.R., 1990. Radiometric considerations for ocean color remote sensors. Applied Optics. 29, 3228–3236.

Haaland, D.M., and Thomas, E.V., 1988. Partial Least-Squares methods for spectral analyses. 1. Relation to other quantitative calibration methods and the extraction of qualitative information. Analytical Chemistry;60:1193–202.

Haenlein, M., Kaplan, A.M., 2004. A beginner's guide to partial least squares analysis. Underst. Stat, 3, 283–297.

Howley, T., Madden, M.G., O'Connell, M.L., Ryder, A.G., 2006. The effect of principal component analysis on machine learning accuracy with high-dimensional spectral data. Knowledge-Based Systems, 19(5), 363-370.

Hugue, F., Lapointe, M., Eaton, B.C., Lepoutre, A., 2016. Satellite-based remote sensing of running water habitats at large riverscape scales: Tools to analyze habitat heterogeneity for river ecosystem management. *Geomorphology*, 253, 353–369.

Jawak, S.D., and Luis, A.J., 2016. High-resolution multispectral satellite imagery for extracting bathymetric information of Antarctic shallow lakes ", Proc. SPIE 9878, Remote Sensing of the Oceans and Inland Waters: Techniques, Applications, and Challenges, 987819: doi:10.1117/12.2222769.

Jordan, D.C., Fonstad, M.A. 2005. Two-dimensional mapping of river bathymetry and power using aerial photography and GIS on the Brazos River, Texas. Geocarto 20(3): 1–8.

Kay, S., Hedley, J.D., and Lavender, S., 2009, Sun Glint Correction of High and Low Spatial Resolution Images of Aquatic Scenes: a Review of Methods for Visible and Near-Infrared Wavelengths, *Remote Sensing*, 1, 697-730.

Kinzel, P.J., Legleiter, C.J., and Nelson, J.M. 2013. Mapping river bathymetry with a small footprint green LiDAR: Applications and challenges. *Journal of the American Water Resources Association*, 49(1): 183-204.

Kirk, J.T.O., 1996.*Light & Photosynthesis in Aquatic Ecosystems*, 2nd ed.; Cambridge University Press: Cambridge, UK.

Lane, S.N., Widdison, P.E., Thomas, R.E., Ashworth, P.J., Best, J.L., Lunt, I.A., Sambrook Smith, G.H., Simpson, C.J., 2010. Quantification of braided river channel change using archival digital image analysis, Earth Surface Processes and Landform, 35(8), pp. 971–985.

Lee, Z.P., Carder, K.L., Mobley, C.D., Steward, R.G., Patch, J.S., 1998, Hyperspectral remote sensing for shallow waters, 1. A semi-analytical model. *Applied Optics*, 37, 6329–6338.

Lee, Z.P., Carder, K.L., Mobley, C.D., Steward, R.G., Patch, J.S., 1999. Hyperspectral remote sensing for shallow waters, 2. Deriving bottom depths and water properties by optimization. *Applied Optics*, 38, 3831–3843.

Legleiter, C.J., 2013. Mapping river depth from publicly available aerial images. River Research and Applications, 29(6): 760-780.

Legleiter, C.J., and Overstreet, B.T. 2012. Mapping gravel-bed river bathymetry from space. *Journal of Geophysical Research - Earth Surface*, 117(F04024): doi: 10.1029/2012jf002539.

Legleiter, C.J., and Overstreet, B.T. 2014. Retrieving river attributes from remotely sensed data: An experimental evaluation based on field spectroscopy at the Outdoor Stream Lab. *River Research and Applications*, 30(6): 671-684.

Legleiter, C.J., and Roberts, D.A., 2009. A forward image model for passive optical remote sensing of river bathymetry. *Remote Sensing of Environment*, 113 (5): 1025-1045.

Legleiter, C.J., Mobley, C.D., and Overstreet, B.T., 2017. A framework for modeling connections between hydraulics, water surface roughness, and surface reflectance in open channel flows. *Journal of Geophysical Research - Earth Surface*, 122(9): 1715-1741.

Legleiter, C.J., Overstreet, B.T., Glennie, C., Zhigang, P., Fernandez-Diaz, J., and Singhania, A. 2016. Evaluating the capabilities of the CASI hyperspectral imaging system and Aquarius bathymetric LiDAR for measuring channel morphology in two distinct river environments. *Earth Surface Processes and Landforms*, 41(3): 344-363.

Legleiter, C.J., Roberts, D.A., and Lawrence, R.L. 2009. Spectrally based remote sensing of river bathymetry. *Earth Surface Processes & Landforms*, 34(8): 1039-1059.

Legleiter, C.J., Roberts, D.A., Marcus, W.A., Fonstad, M.A., 2004. Passive optical remote sensing of river channel morphology and in-stream habitat: Physical basis and feasibility.*Remote Sensing of Environment*,93,493-510.

Legleiter, C.J., Stegman, T.K., and Overstreet, B.T. 2016. Spectrally based mapping of riverbed composition. Geomorphology, 264: 61-79.

Lesser, M.P., Mobley, C.D., 2007, Bathymetry, water optical properties, and benthic classification of coral reefs using hyperspectral remote sensing imagery. *Coral Reefs*, 26, 819–829.

Li, X., Zhang, Y., Bao, Y., Luo, J., Jin, X., Xu, X., Song, X., and Yang G., 2014. Exploring the Best Hyperspectral Features for LAI Estimation Using Partial Least Squares Regression. *Remote Sensing*, *6*, pp. 6221-6241.

Louchard, E.M., Reid, R.P., Stephens, F.C., Davis, C.O., Leathers, R.A., Valerie, D.T., 2003. Optical remote sensing of benthic habitats and bathymetry in coastal environments at Lee Stocking Island, Bahamas: A comparative spectral classification approach. *Limnology and Oceanography*, 48 (2003), pp. 511–521.

Lyzenga, D.R., 1978. Passive remote sensing techniques for mapping water depth and bottom features. *Applied Optics*, 17, 379–383.

Lyzenga, D.R., 1981, Remote sensing of bottom reflectance and water attenuation parameters in shallow water using aircraft and Landsat data, *International Journal of Remote Sensing*, 2:1, 71-82.

Lyzenga, D.R., 1985. Shallow-Water Bathymetry Using Combined Lidar and Passive Multispectral Scanner Data. *International Journal of Remote Sensing*, 6, 115-125.

Lyzenga, D.R., Malinas, N.P. and Tanis, F.J., 2006. Multispectral bathymetry using a simple physically based algorithm, *IEEE Transactions on Geoscience and Remote Sensing*, 44(8), 2251-2259.

Marcus, W. A., and Fonstad, M.A., 2008. Optical remote mapping of rivers at sub-meter resolutions and watershed extents, *Earth Surface Processes & Landforms*, 33(1), 4–24.

Marcus, W. A., and Fonstad, M.A., 2010. Remote sensing of rivers: The emergence of a subdiscipline in the river sciences, *Earth Surface Processes & Landforms*, 35(15), 1867–1872.

Markovitch, S., and Rosenstein, D., 2002, Feature Generation Using General Constructor Functions, *Machine Learning*, 49, 59–98.

Martens, H.A., Dardenne, P., 1998. Validation and verification of regression in small data sets, *Chemometrics and Intelligent Laboratory Systems*, 44, pp. 99–121.

MATLAB, 2018, MATLAB User's Guide. The Math Works, Inc., Natick, MA.

Mobley, C.D., 1994. Light and water: Radiative transfer in natural waters. Academic: San Diego, USA.

Mobley, C.D., and Sundman, L.K., 2008. Hydrolight 5, Ecolight5 User Guide, Sequoia Scientific, Inc., Bellevue.

Montgomery, D.R.,Buffington, J.M.,Smith, R.D., Schmidt, K.M., and Pess, G., 1995. Pool spacing in forest channels. *Water Resources Research*, 31(4), 1097-1105.

Mouw, C.B., Greb, S., Aurin, D.A., DiGiacomo, P.M., Lee, Z., Twardowski, M., Binding, C., Hu, C., Ma, R., Moore, T., Moses, W., Craig, S.E., 2015. Aquatic color radiometry remote sensing of coastal and inland waters: challenges and recommendations for future satellite missions. Remote Sens. Environ. 160, 15–30, http://dx.doi. org/10.1016/j.rse.2015.02.001.

Mumby, P. J., and Edwards, A. J., 2000. Water column correction approaches. In E. P. Green, P. J. Mumby, A. J. Edwards, & C. D. Clark (Eds.), Remote sensing handbook for tropical coastal management. Paris: Unesco. 316 pp.

Niroumand-Jadidi, M. and Vitti, A., 2016, Optimal Band Ratio Analysis of WorldView-3 Imagery for Bathymetry of Shallow Rivers (case Study: Sarca River, Italy), ISPRS - International Archives of the Photogrammetry, Remote Sensing and Spatial Information Sciences, Volume XLI-B8, 2016, pp. 361-364.

Niroumand-Jadidi, M. and Vitti, A., 2017b. Grain Size Mapping in Shallow Rivers Using Spectral Information: A Lab Spectroradiometry Perspective, Proc. SPIE 10422, Remote Sensing of the Ocean, Sea Ice, Coastal Waters, and Large Water Regions 2017, 104220B.

Niroumand-Jadidi, M., and Vitti, A., 2017a. Reconstruction of river boundaries at sub-pixel resolution: Estimation and spatial allocation of water fractions. *ISPRS International Journal of Geo-Information*, 6, 383.

Overstreet, B.T., and Legleiter, C.J. 2017. Removing sun glint from optical remote sensing images of shallow rivers. *Earth Surf Processes & Landforms*, 42(2): 318-333.

Pacifici, F., 2016. Atmospheric Compensation in Satellite Imagery. US Patent 9396528B2.

Pacifici, F., Longbotham, N., and Emery, W. J., 2014. The Importance of Physical Quantities for the Analysis of Multitemporal and Multiangular Optical Very High Spatial Resolution Images, *IEEE Transactions on Geoscience and Remote Sensing*, 52(10),6241-6256.

Pahlevan, N., Roger, J.-C., Ahmad, Z., 2017. Revisiting short-wave-infrared (SWIR) bands for atmospheric correction in coastal waters. Optics Express, 25 (2017), pp. 6015-6035.

Philpot, W. D. 1989. Bathymetric mapping with passive multispectral imagery. Applied Optics, 28: 1569–1578.

Qian, Y., Ye, M., and Zhou, J., 2012, Hyperspectral Image Classification Based on Structured Sparse Logistic Regression and Three-Dimensional Wavelet Texture Features, IEEE Transactions on Geoscience and Remote Sensing, VOL. 51, NO. 4, 2276-2291.

Reunanen, J., 2003. Overfitting in Making Comparisons Between Variable Selection Methods. *Journal of Machine Learning Research*, 3, 1371-1382.

Shintani C., and Fonstad, M.A., 2017. Comparing remote-sensing techniques collecting bathymetric data from a gravel-bed river, *International Journal of Remote Sensing*, DOI: 10.1080/01431161.2017.1280636.

Stumpf, R. P., Holderied, K., and Sinclair, M., 2003. Determination of water depth with high-resolution satellite imagery over variable bottom types. *Limnology and Oceanography*, 48, pp. 547–556.

Walther, S.C., Marcus, W.A., Fonstad, M.A., 2011. Evaluation of high resolution, true colour, aerial imagery for mapping bathymetry in a clear water river without ground-based depth measurements. *International Journal of Remote Sensing*, 32 (15), pp. 4343–4363.

Westaway, R.M., Lane, S.N., and Hicks, D.M., 2001. Airborne remote sensing of clear water, shallow, gravel-bed rivers using digital photogrammetry and image analysis. Photogrammetric Engineering and Remote Sensing, 67: pp. 1271–1281.

Winterbottom, S. J., and Gilvear, D. J., 1997. Quantification of channel bed morphology in gravel-bed rivers using airborne multispectral imagery and aerial photography, *Regulated Rivers: Research & Management*, 13(6), 489–499.

Wold, S., Sjostrom, M., and Eriksson, L., 2001. PLS-regression: a basic tool of chemometrics, Chemometrics and Intelligent Laboratory Systems, 58(2), 109–130.

Woodget, A.S., Carbonneau, P.E., Visser, F., and Maddock, I.P., 2015. Quantifying submerged fluvial topography using hyperspatial resolution UAS imagery and structure from motion photogrammetry. Earth Surface Processes and Landforms, 40: 47–64.